

Full Paper

Influence of Shielding Arrangement on ECT Sensors

A. Martinez Olmos^{1,*}, **J. Alberdi Primicia**² and **J. L. Fernandez Marron**³

1 ETSI Informática, Universidad de Granada. C/ Periodista Daniel Saucedo s/n ,18071, Granada, Spain; Email: amartinez@ugr.es

2 CIEMAT. Avda. Complutense 22, 28040 Madrid, Spain; Email: j.alberdi@ciemat.es

3 ETSI Informática, UNED. C/ Juan del Rosal 16, 28040, Madrid, Spain; E-mail: jlmarron@dia.uned.es

* Author to whom correspondence should be addressed. E-mail: amartinez@ugr.es

Received: 15 May 2006 / Accepted: 21 September 2006 / Published: 22 September 2006

Abstract: This paper presents a full 3D study of a shielded ECT sensor. The spatial resolution and effective sensing field are obtained by means of Finite Element Method based simulations and are compared to a conventional sensor's characteristics. An effective improvement was found in the sensitivity in the pipe cross-section, resulting in enhanced quality of the reconstructed image. The sensing field along the axis of the sensor also presents better behaviour for a shielded sensor.

Keywords: Electrical Capacitance Tomography sensor, Finite Element Method, shielding arrangement, standing capacitance, sensitivity map, sensing field, reconstructed image

1. Introduction

In the recent years, Electrical Capacitance Tomography (ECT) and Electrical Impedance Tomography (EIT) have been widely used to image and control flow processes involving several phases, such as gas-oil, water-oil, sand-air, and so on... [1-3].

These techniques are used to obtain information about the spatial distribution of a mixture of materials inside a vessel, by measuring the electrical capacitances or resistances between sets of electrodes placed around its periphery and converting them into an image showing the distribution of permittivity or resistivity, respectively, by means of tomography data processing. The quality of the reconstructed image depends on the sensor configuration, since it determines the resolution and effective sensing field of the system.

Finite Element Method (FEM) based simulations have prove to be useful tools for studying the sensitivity of ECT and EIT sensors [4-6] and can therefore be applied to obtain optimum designs.

In this paper, a in-house FEM software package is used to characterize a shielded ECT sensor, which has a grounded isolation around every measurement electrode and driven guard (see Figure 1 (a)). The resolution obtained in the cross-section of the pipe and along the Z axis is compared to conventional non-shielded sensor resolution.

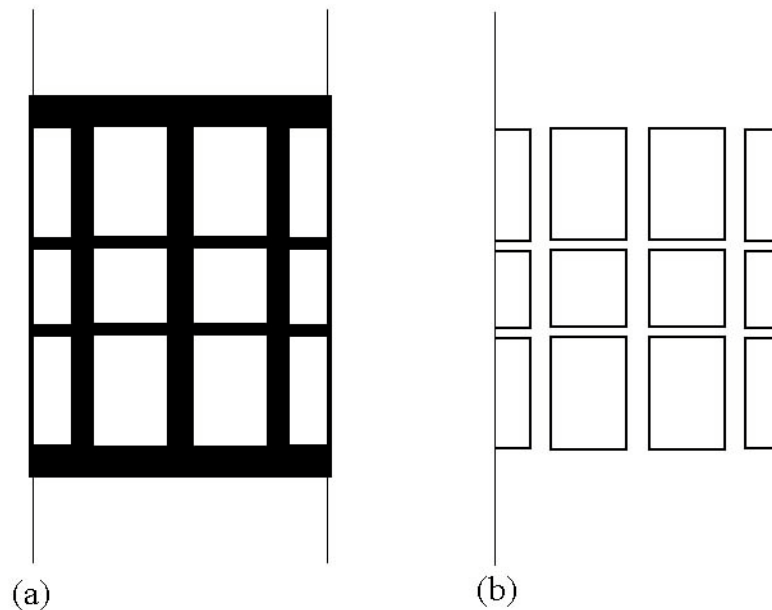


Figure 1. ECT sensor configurations: (a) with grounded shielding and (b) without shielding.

The FEM software is aimed at solving both the forward and the inverse problems. The forward problem is to obtain the set of capacitances between all the different electrode pairs, for a given permittivity distribution. In contrast the inverse problem is to obtain the permittivity distribution, that is, the reconstructed image, from a set of measured capacitances. To solve both problems, relationship (1) is used, with appropriate Dirichlet conditions.

$$C = \frac{Q}{V} = -\frac{1}{V} \iint_{\Gamma} \varepsilon(x, y, z) \nabla \varphi(x, y, z) d\Gamma \quad (1)$$

where $\varepsilon(x, y, z)$ is the permittivity distribution inside the pipe, $\varphi(x, y, z)$ is the potential distribution and Γ is the electrode surface.

The mesh used to apply the FEM scheme is shown in Figure 2. This mesh is repeated along the Z axis.

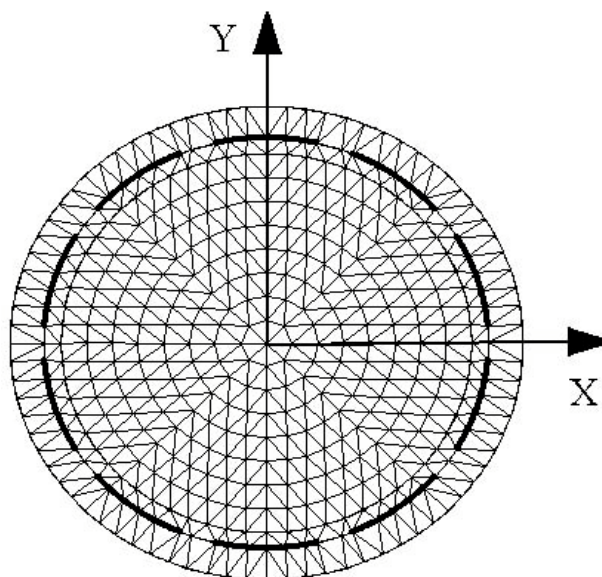


Figure 2. 2D mesh.

The system used here consists of a sensor with 10 measurement electrodes and two sets of driven guards. The electrode size is 3 cm x 3 cm. Guard length is 5 cm, inner radius is 6 cm, and outer radius is 6.5 cm. An external grounded screen surrounds the sensor, with a radius of 7.5 cm. The pipe wall is assumed to have a relative permittivity of 2.8.

2. Numerical results

The main effect of the grounded shield is to confine the field lines within the pipe, so that they cannot travel from the source electrode to the measuring electrode through the pipe wall, as shown in Figure 3.

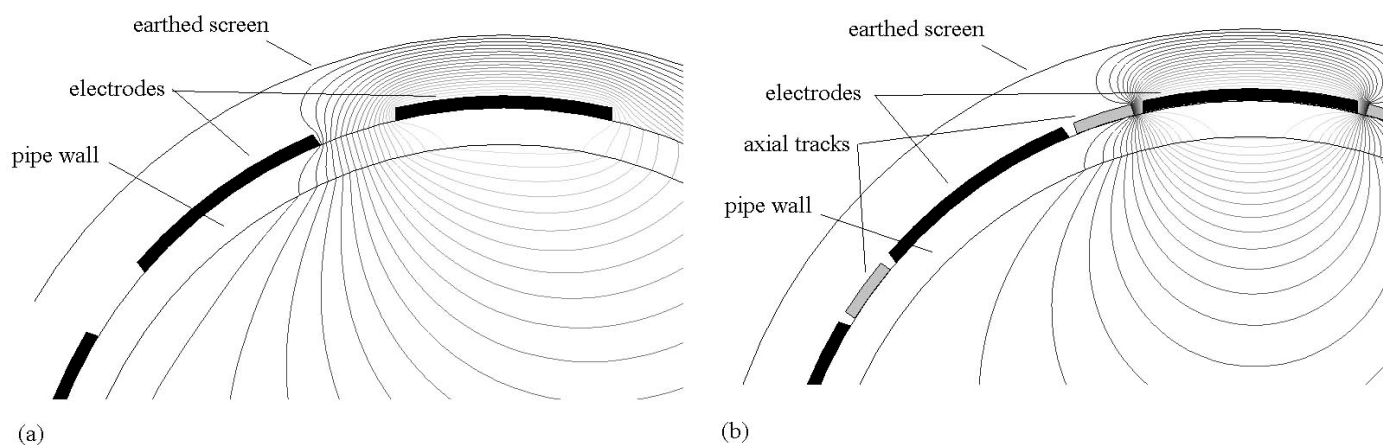


Figure 3. Equi-potential lines in the cross section for: (a) non-shielded sensor and (b) shielded sensor.

As can be seen, the field lines that travel from the source electrode through the pipe wall, crossing the equi-potential lines perpendicularly, die at the grounded axial tracks before they can reach the measuring electrode. The external field lines are neutralized by the grounded screen. Consequently, the capacitance measured between these electrodes is due only to the field lines that cross the dominion under study, i.e., the interior of the pipe.

This reduction in the field lines that reach the measurement electrode causes a decrease in the accumulated charge in the electrode that results in a lower capacitance. Figure 4 shows the standing capacitances when the pipe is full of air for a shielded and a non-shielded sensor.

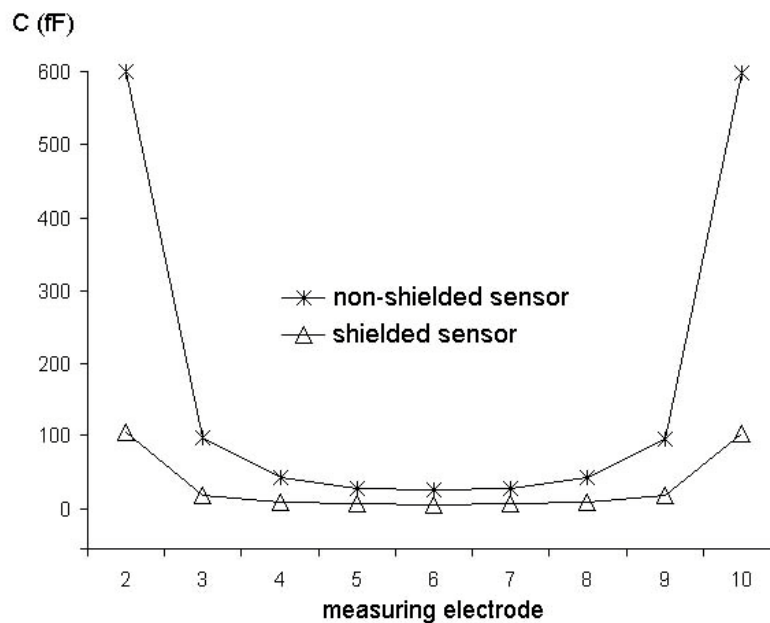


Figure 4. Standing capacitances for a shielded and a non-shielded sensor. Source electrode is number 1.

The sensitivity map for an electrode pair i - j is given by equation (2).

$$S_{ij}(e) = \frac{C_{ij}(e) - C_{ij}^l}{C_{ij}^h - C_{ij}^l} \cdot \frac{1}{\varepsilon^h - \varepsilon^l} \cdot \mu(e) \quad (2)$$

where $C_{ij}(e)$ is the capacitance between electrodes i - j when every element inside the pipe has a permittivity of ε^l (lowest value) except for element e , which has a high value of permittivity ε^h , C_{ij}^l is the capacitance between electrodes when the medium inside the pipe has low permittivity, and C_{ij}^h is the capacitance when the medium has high permittivity. The parameter $\mu(e)$ is a scale factor related to the area or volume of the element.

The sensitivity maps at $z=0$ for the different electrode pairs are affected by the shielding arrangement. Figure 5 depicts a comparison between sensitivity maps for several electrode pairs in shielded and non-shielded sensors.

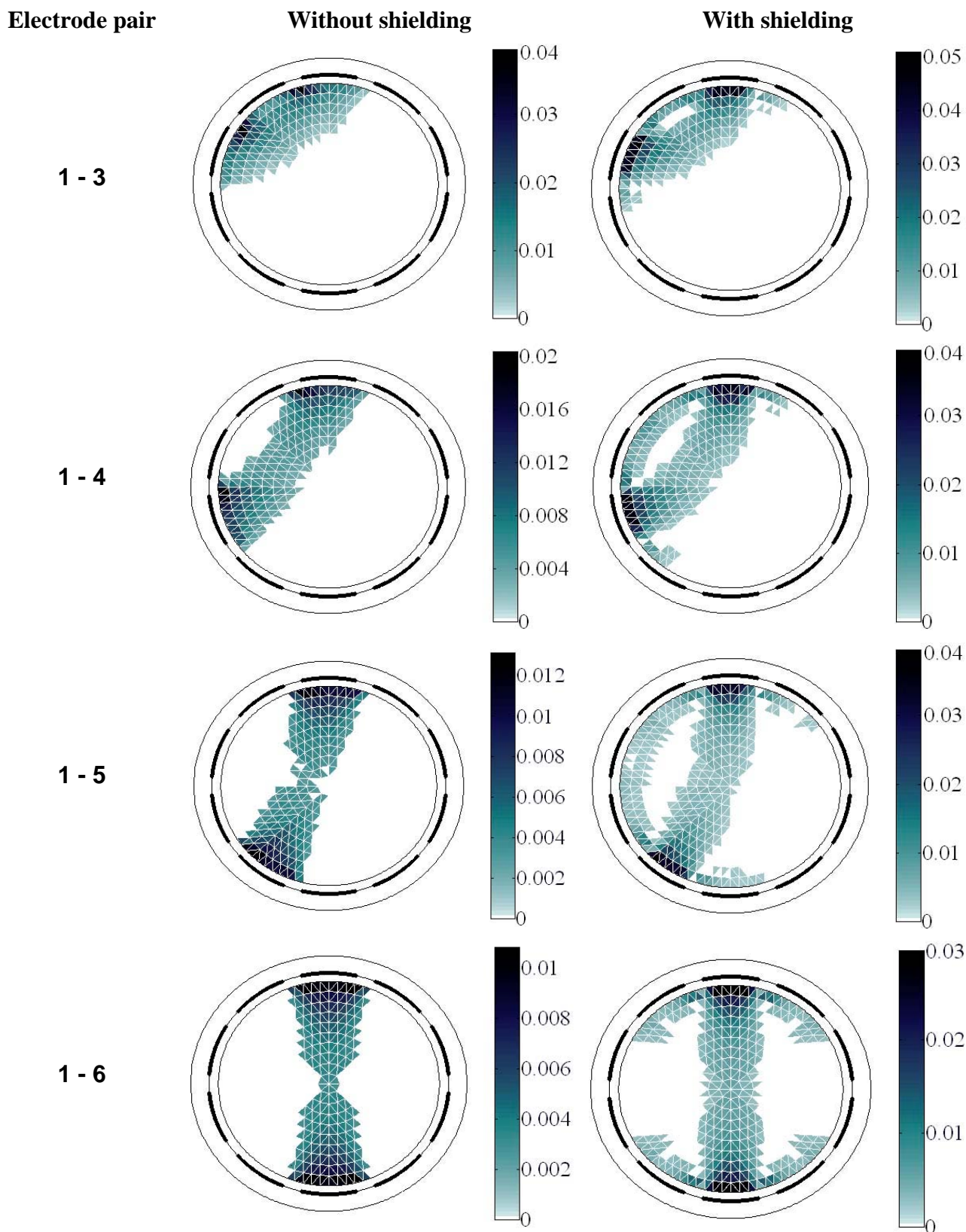


Figure 5. Sensitivity maps in a non-shielded sensor and a shielded sensor for different electrode pairs.

Figure 5 indicates that the sensitivity is higher, in absolute terms, when a shielding arrangement is used, and that the sensing area for every electrode pair [7] is improved. Moreover, in the shielded sensor the highest sensitivity is found close to all the electrode surfaces, and not only near the edges, as happens in the non-shielded sensor.

The electric field distribution along the Z axis also becomes distorted when grounded shielding is present. Figure 6 shows how the equi-potential lines are affected by the influence of the grounded tracks between the measurement electrode and the driven guards.

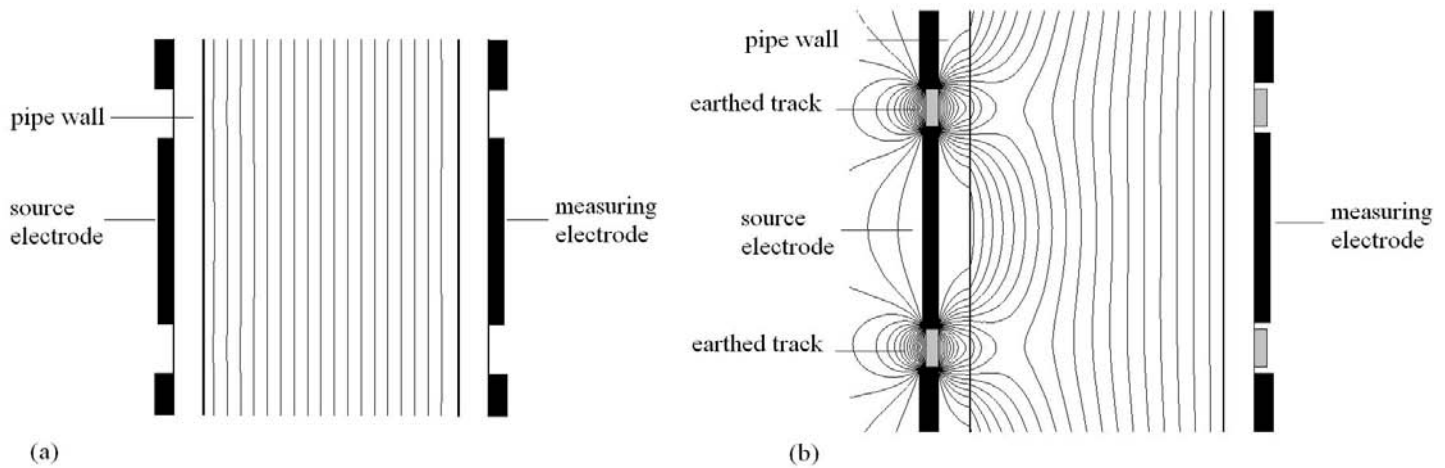


Figure 6. Equi-potential lines along Z axis in a: (a) non-shielded sensor and (b) shielded sensor.

This distortion has a direct effect upon the effective sensing field. To check the influence of the shielding arrangement on the Z-detection maps [7], the sensitivity of adjacent and opposite electrodes along the Z axis was calculated at three typical test elements shown in Figure 7.

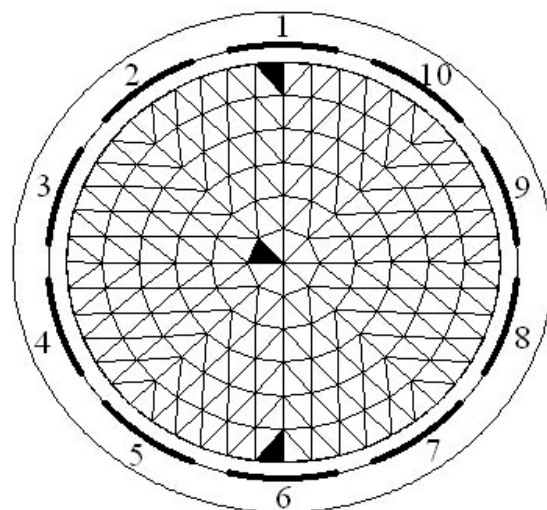


Figure 7. Test elements.

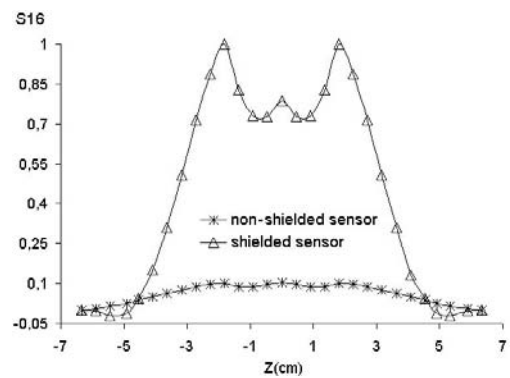
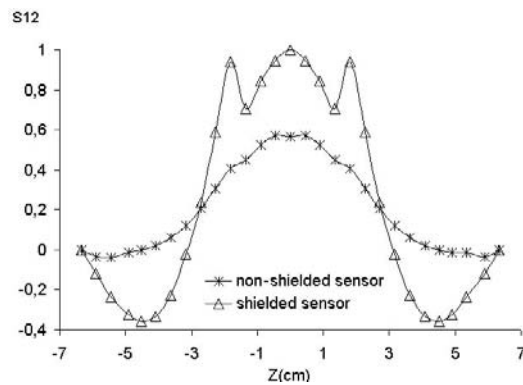
The detection maps (normalized sensitivity maps) along the Z axis obtained are presented in Figure 8.

Test element

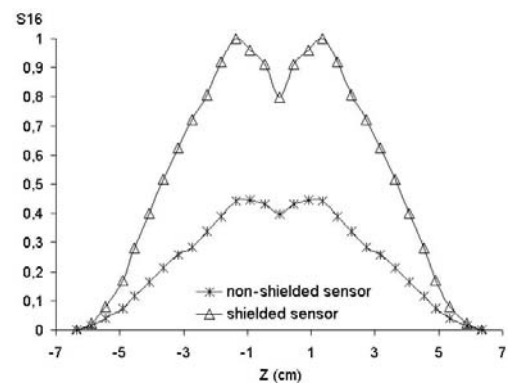
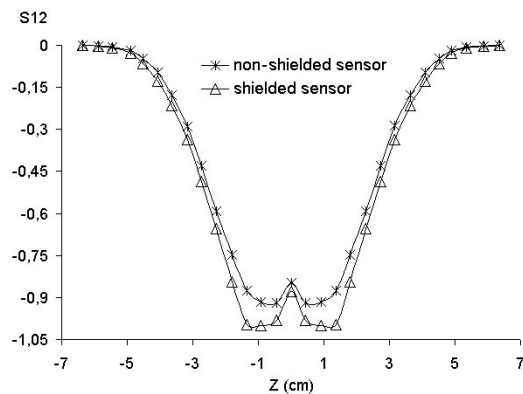
Adjacent electrodes 1 and 2

Opposite electrodes 1 and 6

Upper



Middle



Lower

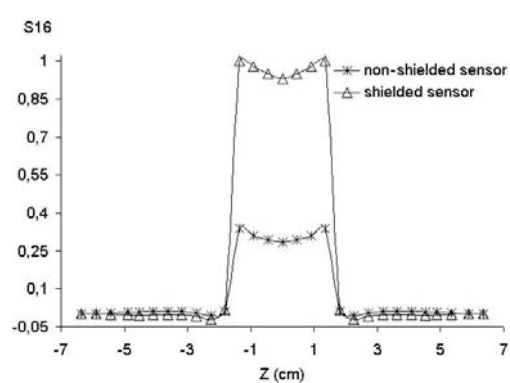
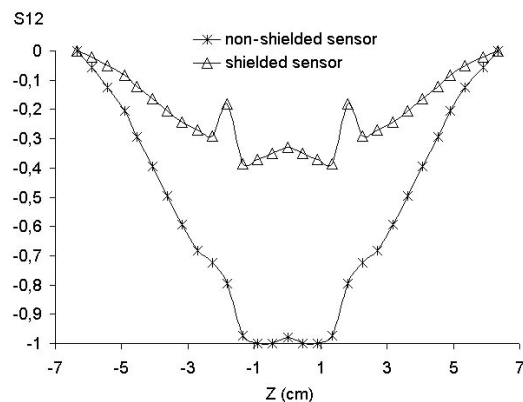


Figure 8. Z-detection maps for adjacent (1-2) and opposite (1-6) electrodes, calculated at the upper, middle and lower test elements.

The effective detection width is narrower near the electrodes for a shielded sensor. For opposite electrodes (right column in Figure 8), the absolute sensitivity is clearly improved when using the grounded shield. For adjacent electrodes, the sensitivity is higher for the shielded sensor only near the source and measurement electrodes and gets worse farther from them. Moreover, the sensitivity shape shows strong shifts near the edges of the electrodes in the shielded sensor, but is smoother in the non-shielded sensor.

3. Image reconstruction

A simulated image reconstruction of objects shown in Figure 9 (a) was carried out with the two sensor schemes. Reconstructed permittivity distribution was obtained using the *singular value decomposition method* to solve (3), where \mathbf{g} is the permittivity vector, \mathbf{S} is the Jacobian matrix of normalized capacitance (i.e. the matrix of sensitivity maps) and $\boldsymbol{\lambda}$ is the normalized capacitance vector.

$$\boldsymbol{\lambda} = \mathbf{S}\mathbf{g} \quad (3)$$

This method provides an approximate solution \mathbf{g}^* by decomposing matrix \mathbf{S} as

$$\mathbf{S} = \mathbf{U}\boldsymbol{\Sigma}\mathbf{V}^T \quad (4)$$

where

$$\begin{aligned} \mathbf{U} &= [\mathbf{u}_1, \mathbf{u}_2, \dots, \mathbf{u}_M] \\ \mathbf{V} &= [\mathbf{v}_1, \mathbf{v}_2, \dots, \mathbf{v}_N] \\ \boldsymbol{\Sigma} &= \text{diag}[\sigma_1, \sigma_2, \dots, \sigma_p] \end{aligned} \quad (5)$$

with the coefficients σ_k being the singular values of \mathbf{S} .

The approximate solution of (3) is then given by:

$$\mathbf{g}^* = \mathbf{V}\boldsymbol{\Sigma}^{-1}\mathbf{U}^T\boldsymbol{\lambda} \quad (6)$$

Reconstructed images for a non-shielded sensor and a shielded sensor are presented in Figures 9 (b) and (c), respectively.

The norms of the original (\mathbf{g}) and obtained (\mathbf{g}^*) permittivity distribution vectors can be used to calculate the relative image error [8]:

$$\text{Image error} = \frac{\|\mathbf{g}^* - \mathbf{g}\|}{\|\mathbf{g}\|} \quad (7)$$

The image error for the first permittivity distribution (Figure 9 (a)) is 1.2267 for the non-shielded sensor, and 0.6933 for the shielded one. For the second permittivity distribution (in Figure 9 (b)), the errors are 0.4583 and 0.289 for the non-shielded and the shielded sensors, respectively.

From these results, it is proved that the reconstructed image quality is better when using a grounded shield.

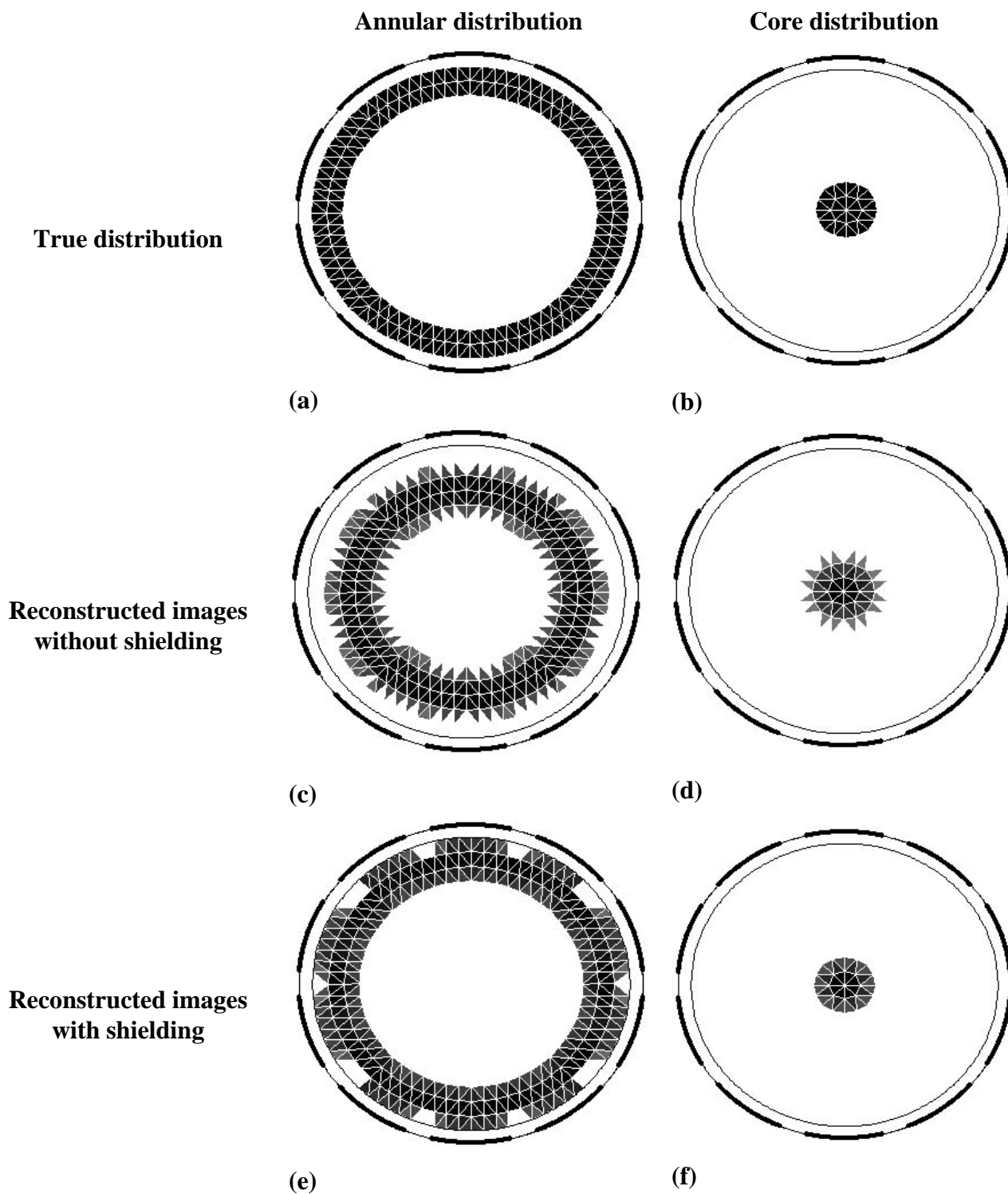


Figure 9: Simulated permittivity distributions (a) and reconstructed image for a shielded and a non-shielded sensor.

4. Conclusions

The scheme of a shielded ECT sensor has been introduced. Finite Element Method based simulations have been carried out in order to study the sensitivity parameters of the shielded sensor,

and the results have been compared to the response of a non-shielded sensor with the same electrode configuration.

The shielded sensor presents better behaviour in the cross-section, with higher absolute sensitivity and broader sensing space. Furthermore, the sensing field was found to improve along the Z axis, especially for opposite electrodes, although a distortion effect arose in the form of shifts near the edges of the electrodes.

The overall effect of the shielding arrangement was checked by simulating two image reconstructions using a singular value decomposition technique. The quality of the image obtained with the shielded sensor was clearly better than that reconstructed with the non-shielded one, in both cases.

The only disadvantage to using a shielded sensor is the lower inter-electrode capacitances to be measured, which might cause a resolution problem when using a certain sensing-electronics.

Acknowledgements

This job was financed for the Spanish Education and Science Ministry with a CICYT grant (reference DPI2002/04550/C07/04).

References and Notes

1. Arko, A.; Waterfall, R. C.; Beck, M. S.; Dyakowski, T.; Sutcliffe, P.; Byars, M. Development of Electrical Capacitance Tomography for Solid Mass Flow Measurement and Control of Pneumatic Conveying Systems. *1st World Congress on Industrial Process Tomography, Buxton, Greater Manchester*, April 14-17, 1999.
2. Scott, D. M.; Gutsche, O. W. ECT Studies of Bead Fluidization in Vertical Mills. *1st World Congress on Industrial Process Tomography, Buxton, Greater Manchester*, April 14-17, 1999.
3. Wang, M.; Yin, W.; Holliday, N. A Highly Adaptative Electrical Impedance Sensing System for Flow Measurement. *Meas. Sci. Technol.* **2002**, *13*, 1884-1889.
4. Yan, H.; Shao, F.Q.; Xu, H.; Wang, S. Three Dimensional Analysis of Electrical Capacitance Tomography Sensing Fields. *Meas. Sci. Technol.* **1999**, *10*, 717-725.
5. Wang, H. X.; Yin, W.; Yang, W.Q.; Beck, M.S. Design of Segmented Capacitance Sensing Array for Multi-phase Interface Measurement. *Meas. Sci. Technol.* **1996**, *7*, 79-86.
6. Polydorides, N.; McCan, H. Electrode Configurations for Improved Spatial Resolution in Electrical Impedance Tomography. *Meas. Sci. Technol.* **2002**, *13*, 1862-1870.
7. Martinez Olmos, A.; Alberdi Primicia, J.; Fernandez Marron, J.L. Simulation Design of ECT. **2006**. To be published.
8. Yang, W. Q.; Peng, L. Image Reconstruction Algorithm for Electrical Capacitance Tomography. *Meas. Sci. Technol.* **2003**, *14*, R1-R13.